

Sea ice thickness retrieval from SMOS high incident angle observations

M. Huntemann et al.

This discussion paper is/has been under review for the journal The Cryosphere (TC). Please refer to the corresponding final paper in TC if available.

Empirical sea ice thickness retrieval during the freeze up period from SMOS high incident angle observations

M. Huntemann¹, G. Heygster¹, L. Kaleschke², T. Krumpen³, M. Mäkynen⁴, and M. Drusch⁵

¹Institute of Environmental Physics, University of Bremen, Germany

²Institute of Oceanography, University of Hamburg, Germany

³Alfred Wegener Institute, Bremerhaven, Germany

⁴Finnish Meteorological Institute, Helsinki, Finland

⁵ESTEC, ESA, Noordwijk, the Netherlands

Received: 30 July 2013 – Accepted: 8 August 2013 – Published: 30 August 2013

Correspondence to: M. Huntemann (marcus.huntemann@uni-bremen.de)

Published by Copernicus Publications on behalf of the European Geosciences Union.

Title Page

Abstract

Introduction

Conclusions

References

Tables

Figures

⏪

⏩

◀

▶

Back

Close

Full Screen / Esc

Printer-friendly Version

Interactive Discussion

Abstract

Sea ice thickness information is needed for climate modeling and ship operations. Here a method to detect the thickness of sea ice up to 50 cm during the freezeup season based on high incidence angle observations of the Soil Moisture and Ocean Salinity (SMOS) satellite working at 1.4 GHz is suggested. By comparison of thermodynamic ice growth data with SMOS brightness temperatures, a high correlation to intensity and an anti correlation to the difference between vertically and horizontally polarised brightness temperatures at incidence angles between 40 and 50° are found and used to develop an empirical retrieval sensitive to thin sea ice up to 50 cm thickness. It shows high correlations with ice thickness data from airborne measurements and reasonable ice thickness patterns for the Arctic freeze up period.

1 Introduction

Sea ice is an essential climate component and observations of its formation, evolution, and decay are important for understanding and predicting climate change. Sea ice coverage has been observed since 1978 using several microwave radiometers, namely the Scanning Multi-channel Microwave Radiometer (SMMR) (1978–1987), Special Sensor Microwave Imager (SSM/I)/Sounder (SSMIS) (1987–today) and Advanced Microwave Scanning Radiometer – Earth Observing System (EOS) (AMSR-E) (2002–2012). The sensitivity of the microwave emission of sea ice has been narrowed down to few essential microphysical properties like sea ice thickness, salinity temperature and snow grain size (Tonboe et al., 2011; Fuhrhop et al., 1998). Since 2009 the ESA SMOS (Soil Moisture and Ocean Salinity) mission, is observing the Earth at 1.4 GHz (L-band), from a sun synchronous dusk-dawn orbit (Kerr et al., 2001). At this frequency, the penetration depth into sea ice is about 50 cm and even more in less saline waters like the Baltic sea.

TCD

7, 4379–4405, 2013

Sea ice thickness retrieval from SMOS high incident angle observations

M. Huntemann et al.

Title Page

Abstract

Introduction

Conclusions

References

Tables

Figures

⏪

⏩

◀

▶

Back

Close

Full Screen / Esc

Printer-friendly Version

Interactive Discussion

Sea ice thickness retrieval from SMOS high incident angle observations

M. Huntemann et al.

Title Page

Abstract

Introduction

Conclusions

References

Tables

Figures

⏪

⏩

◀

▶

Back

Close

Full Screen / Esc

Printer-friendly Version

Interactive Discussion



Figure 1 (left) illustrates the basic situation: the brightness temperature of open water at nadir is around 100 K. For vertical polarisation, it increases with incidence angle up to 180 K at 65°, and for horizontal polarisation it decreases down to about 60 K. At all incidence angles, the signal of sea ice is clearly higher. The vertically polarised emission increases from 230 K at nadir to 260 K at 65°, and the horizontally polarised emission decreasing down to 215 K. The high dynamic range from open water to sea ice of over 100 K encourages us to investigate the sea ice growth process with increasing sea ice thickness as reflected in the L-band emission, and to explore the potential to retrieve the thickness of the growing sea ice from the SMOS observations. Kaleschke et al. (2009, 2012) first showed that for nadir observations of up to 40° incident angle, the intensity can be used to obtain information on the sea ice thickness.

In this paper we use the radiation at higher incidence angles between 40° and 50° which allows to exploit in addition to the intensity the polarisation difference, the difference between the intensities observed at vertical and horizontal polarisation. As a consequence, this method will be based on data completely independent of those used by Kaleschke et al. (2012).

2 SMOS data source and processing

The instrument Microwave Imaging Radiometer with Aperture Synthesis (MIRAS) onboard of the SMOS satellite provides data since 2010 (Mecklenburg et al., 2012). Each of its 69 receivers, organized along the shape of a three-leg star, takes radiances from which brightness temperatures are determined. The unit of data processed in one aperture synthesis step is called a snapshot (Fig. 2), a set of about 100 × 100 brightness temperatures generated from the initial observations by essentially correlating the signals from the 69 receivers amongst each other and applying a Fourier like back transform (Corbella et al., 2004). Each 1.2 s, one snapshot is taken

We are using two types of input data, SMOS Level 1C data and Binary Universal Form for the Representation of meteorological data (BUFR). In both input formats the

Sea ice thickness retrieval from SMOS high incident angle observations

M. Huntemann et al.

Title Page

Abstract

Introduction

Conclusions

References

Tables

Figures

⏪

⏩

◀

▶

Back

Close

Full Screen / Esc

Printer-friendly Version

Interactive Discussion

data is provided gridded in the Icosahedron Snyder Equal Area (ISEA) 4H9 grid (Sahr et al., 2003), an equal area grid. The gridding introduces positional errors of few kilometers, which are not critical since the SMOS footprint with its size at nadir about $30 \times 30 \text{ km}^2$, increasing with incident angle up to $90 \times 33 \text{ km}$ at about 65° , is much larger. As each footprint overlaps several grid points (Castro, 2008), the data of neighbouring grid points are correlated.

The L1C data cover the whole ISEA 4H9 Discrete Global Grid (DGG), but are available at about 24 to 48 h delay. As for operational sea ice services, a shorter delay is required, the BUFR data, offering SMOS data with only 3 to 4 h delay, are used. In order to reduce the data volume, over ocean in the BUFR data only each second DGG cell is represented.

Even though the frequency band near 1.4 GHz is not allowed for communication, there were man-made emissions during the early phase of the SMOS mission (Camps et al., 2010), so that the data acquired was highly influenced by Radio Frequency Interference (RFI) (Oliva et al., 2012), even in the polar regions. The RFI-influenced data shows mostly higher brightness temperature (T_b) than occur in nature. All surface emissions of more than $T_b = 300 \text{ K}$ are unrealistic because they would require an emissivity larger than unity and are taken as RFI. Due to the Fourier transform like reconstruction of the snapshots, the RFI from a single source on earth may extend over the whole snapshot, albeit at lower values. In order to also discard lower RFI influences, in our processing the whole snapshot is sorted out if at least one pixel shows a brightness temperature larger than 300 K. An example of RFI can be seen in the snapshot in Fig. 2.

During the investigation period October to December 2010, SMOS was operating in full polarisation mode, i.e. measuring all four Stokes components. However, these are delivered in the L1C and BUFR data sets with respect to the instrument reference plane (X, Y) and need to be converted to the earth surface plane (V, H) by the transformation

Sea ice thickness retrieval from SMOS high incident angle observations

M. Huntemann et al.

$$\begin{bmatrix} A_1 \\ A_2 \\ A_3 \\ A_4 \end{bmatrix} = \begin{bmatrix} \cos^2(\alpha) & \sin^2(\alpha) & -\cos(\alpha)\sin(\alpha) & 0 \\ \sin^2(\alpha) & \cos^2(\alpha) & \cos(\alpha)\sin(\alpha) & 0 \\ \sin(2\alpha) & -\sin(2\alpha) & \cos(2\alpha) & 0 \\ 0 & 0 & 0 & 1 \end{bmatrix} \begin{bmatrix} TB_H \\ TB_V \\ TB_3 \\ TB_4 \end{bmatrix} \quad (1)$$

with $A_1 = \Re(TB_{XX})$, $A_2 = \Re(TB_{YY})$, $A_3 = 2\Im(TB_{XY})$, $A_4 = -2\Im(TB_{XY})$ and $\alpha = \alpha_r + \omega_{F\alpha}$ where α_r and $\omega_{F\alpha}$ are geometric rotation angle and Faraday rotation angle, respectively, which are supplied in the SMOS L1C and BUFR data. $\Re(\dots)$ and $\Im(\dots)$ are the real and imaginary part, respectively.

The transformation needs for each observation in the (V, H) frame brightness temperatures at three polarisations: XX , YY and XY . However, only one (either XX or YY) or two of them (either (XX, XY) or (YY, XY)) are measured within one snapshot so that either one or two missing values need to be interpolated.

We use observations from neighbouring, overlapping snapshots acquired within 2.5 s before or after the time of interest (SMOS takes snapshots every 1.2 s). Within 2.5 s the atmosphere and surface conditions should change only little. If no suitable values for interpolation can be found, this observation is discarded from the transformation and further data analysis. As an additional condition, the incidence angle may only vary less than 0.5° , which ensures the accuracy of the interpolation since the polarised brightness temperatures vary quite strong at the considered incident angles (Fig. 1).

3 Sea ice thickness retrieval method

The first step to develop a fully empirical retrieval was to get training data and analyse it for consistency. Since Sea Ice Thickness (SIT) of thin ice during the freeze up period is hard to observe in situ (one cannot stand or walk on it), we had to rely on other, model based sources as ground truth:

[Title Page](#)
[Abstract](#)
[Introduction](#)
[Conclusions](#)
[References](#)
[Tables](#)
[Figures](#)
[⏪](#)
[⏩](#)
[◀](#)
[▶](#)
[Back](#)
[Close](#)
[Full Screen / Esc](#)
[Printer-friendly Version](#)
[Interactive Discussion](#)

Sea ice thickness retrieval from SMOS high incident angle observations

M. Huntemann et al.

Title Page

Abstract

Introduction

Conclusions

References

Tables

Figures

⏪

⏩

◀

▶

Back

Close

Full Screen / Esc

Printer-friendly Version

Interactive Discussion



- The one-dimensional HIGH-resolution Thermodynamic Snow/Ice model (HIGHTSI) (Launiainen and Cheng, 1998), a regional thermodynamic one dimensional sea ice growth model driven by High Resolution Limited Area Model (HIRLAM), (Källen, 1996; Unden et al., 2002), a short-range weather forecasting system intended to use for limited areas developed by eleven European countries (<http://www.hirlam.org>)
- Towards an Operational Prediction system for the North Atlantic European coastal Zones (TOPAZ) (Sakov et al., 2012), a coupled ocean-sea ice data assimilation system which, among other, provides information on sea ice thickness and sea ice concentration.
- National Centers for Environmental Prediction (NCEP) and National Center for Atmospheric Research (NCAR) produce Analysis/Reanalysis data out of observations and historic data, frequently used as reference for global climate variables and for initializing mesoscale atmospheric models. The spatial resolution is 2.5°.
- European Centre for Medium-Range Weather Forecasts (ECMWF) Re-Analysis (ERA) data is like NCEP data out of observations and modeled data. The resolution is 1.5°.

While TOPAZ and HIGHTSI contain the SIT directly, NCEP and ECMWF can only be used to calculate the SIT using the air temperature as input for the Cumulative Freezing Degree days (CFDD) model (Bilello, 1961; Weeks, 2010):

$$\text{SIT}[\text{cm}] = 1.33 \cdot (\text{CFDD}[\text{°C}])^{0.58} \quad (2)$$

where CFDD is the daily average temperature below the freezing point of sea water (−1.8°C), integrated over the time period since first sea ice has been formed at this point and in this ice season.

Because of the region covered by HIGHTSI we chose ten grid cells in the Kara and Barents sea shown in Fig. 3. The time is restricted to the period of strongest

Sea ice thickness retrieval from SMOS high incident angle observations

M. Huntemann et al.

Title Page

Abstract

Introduction

Conclusions

References

Tables

Figures

◀

▶

◀

▶

Back

Close

Full Screen / Esc

Printer-friendly Version

Interactive Discussion

yield ice concentrations below 100 % in case of a thin ice cover. In order not to miss these initial ice thicknesses, we include observations with the initial increase of ice concentration from 0 to 100 % (days 20 to 29 in Fig. 4) into the training data set while later drops in SIC, possibly caused by wind induced ice breakups, are excluded (days 30 to 32 in Fig. 4). Excluded areas are shaded grey in Fig. 4. Similar investigations have been carried out for all 10 regions of Fig. 3 (Heygster et al., 2012)

The Stokes components obtained from the sensor are converted into intensity I and polarisation difference Q . Empirical functions are fitted to these parameters varying with SIT obtained from the models for each of the different training areas using the fit functions are

$$I_{abc}(x) = a - (a - b) \cdot \exp(-x/c) \quad (3)$$

$$Q_{abcd}(x) = (a - b) \cdot \exp(-(x/c)^d) + b. \quad (4)$$

Equation (3) is also used in Kaleschke et al. (2012) and is basically the Lambert-Beer law. Equation (4) was chosen empirically since it allows to represent the shape of thickness dependence of the polarisation difference in an appropriate way

For training, only the CFDD derived SIT from NCEP data is used, so that the HIRLAM driven Moderate-resolution Imaging Spectroradiometer (MODIS) observations may serve in the next section as independent validation data. Since HIGHTSI is also driven by HIRLAM, HIGHTSI data is not used for training of the retrieval. Table 1 shows the optimal parameters which best represents the training data set.

Figure 5 shows the two functions as a parameterized curve in the (Q, I) plane. The color of the points indicates the different regions (Fig. 3). The curved, black line represents the SIT retrieved for a given pair (Q, I) . For finding the SIT for given I and Q , the minimum Euclidean distance to the retrieval curve is determined. Figure 5 shows that changes in Q only influence the retrieved SIT at higher intensities i.e. SIT higher than 30 cm. At higher SIT the returned values are sensitive to the observed brightness temperatures I and Q of which the uncertainty is up to 5 K for the incident angles of 40° to 50° , similar to the estimate by Kaleschke et al. (2012). Therefore the retrieval is cut

off at 50 cm SIT. Higher retrieved values are marked by a flag for more than 50 cm but no distinct values are returned.

It should be mentioned that the retrieval in the present form assumes ice concentrations of 100 %. Introducing a second observation Q in the retrieval would in principle allow to determine simultaneously a second parameter, e.g. the ice concentration. An example observations $P = (Q, I)$ (Fig. 5) then could be explained as a linear combination of open water (ice thickness 0 cm) and 40 cm thick ice. However, attempts to establish such a two-parameter retrieval have turned out to be quite noisy (Heygster et al., 2012). Therefore, here we refrain from a two-parameter retrieval. The advantage of introducing a second parameter is rather a gain of sensitivity in the upper range of ice thicknesses. While above 30 cm the intensity I changes only little with thickness, the polarisation difference Q contains enough sensitivity to expand the retrieval up to 50 cm (Fig. 5).

3.1 Error estimation

For each 10 cm interval of the NCEP CFDD SIT, the RMSD to the SIT retrieved from SMOS is shown in Table 2. The error is about 30 % of the retrieved value. The retrieval of very thin ice of 0 to 20 cm is quite accurate and stable. Higher retrieved SIT have a larger error and because of the restriction of the SIT retrieval to 50 cm, it might yield larger deviations close to the 50 cm border. The margins in Table 2 describe how well the retrieval curve represents the learning data set based on the NCEP CFDD data. It includes the errors introduced by the NCEP and CFDD models and by sea ice drift. In the next chapter the retrieved SIT values will be compared to independent SIT values, making the error characterization independent of the used learning data set.

Sea ice thickness retrieval from SMOS high incident angle observations

M. Huntemann et al.

Title Page

Abstract

Introduction

Conclusions

References

Tables

Figures



Back

Close

Full Screen / Esc

Printer-friendly Version

Interactive Discussion

4 Validation

4.1 With MODIS thermal imagery SIT retrieval

25 SIT data from MODIS nighttime thermal imagery (Yu and Rothrock, 1996; Mäkynen, 2011) is used to validate the SMOS algorithm. Since MODIS has a much higher horizontal resolution than SMOS, the MODIS data have to be averaged to the SMOS resolution. Another inherent discrepancy between the two data sets is that, when calculating the SMOS SIT, the data of one day is averaged while the MODIS data stem
5 from single overflights.

The SMOS and MODIS SIT retrievals from 4 December 2010 are shown in Fig. 6 (top left and top center). The MODIS image shows incomplete coverage due to clouds. Some regions like North West of Novaya Zemlya show a good agreement in shape and thickness distribution of the sea ice. In the image center, East and South of the
10 North East tip of Novaya Zemlya, SMOS retrieves higher SIT values than MODIS. Areas closer to the coast than 40 km are screened out in the SMOS retrieval because of potential land influence. In Fig. 6 (top right) the averaged MODIS SIT values suitable for comparison with SMOS SIT are shown. Figure 6 (bottom) shows the scatter plot of the MODIS and SMOS SIT retrievals. The different colors represent the standard deviation of the averaged MODIS data over one SMOS footprint. Low standard deviations,
15 i.e., more homogeneous ice thickness according to MODIS, tend to give the highest correlation with the large-footprint SMOS retrieved SIT. At lower SIT, SMOS retrieves higher SIT than MODIS. For the linear regression all points were excluded where either SMOS or MODIS showed SIT larger than 50 cm as indicated by the shaded areas
20 (Fig. 6, bottom). The correlation of both retrievals is $r = 0.82$. Two more scenes have been analyzed with similar results by Heygster et al. (2012).

For the assessment of the comparison with MODIS derived SIT it should be kept in mind that the MODIS SIT yields errors of mostly 40–50 % (Mäkynen et al., 2013). While the good agreement of SIT from both sensors below 20 cm thickness supports
25 the conclusion of lower errors in this range (Table 2), we cannot attribute the statistic

disagreement at higher thicknesses to any of the two sensors. In addition, the errors in the two retrievals stem from different sources. While the SMOS brightness temperatures are expected to have a higher random error due to lower radiometric accuracy while the atmosphere is close to transparent, MODIS radiances may be influenced by thin clouds missed by the MODIS cloud mask.

4.2 With EM bird airborne measurements

The Alfred Wegener Institut (AWI) has developed an airborne instrument to measure SIT when attached to a plane or helicopter (Haas et al., 2009), called EM bird. It uses the conductivity of water and a laser altimeter to get the height difference between the top and bottom layer of the sea ice. The SITs are determined at an absolute error of less than 10 cm for a single measurement. For freshly frozen thin sea ice, the EM bird might underestimate the SIT since its conductivity is higher due to the higher salinity. Therefore, in regions like the Laptev sea known for high variations in salinity trough the year, the insufficient knowledge of the salinity can induce a higher error (Krumpen et al., 2012). However, when averaged over spatial scales of a SMOS footprint, we expect the EM bird to deliver valuable validation data. On 20 April 2012 an EM bird measurement in the Laptev sea was taken over freshly frozen thin sea ice with negligible snow cover, shown in Fig. 7 together with the SMOS retrieval. For each EM bird dot in Fig. 7 (left), 250 measurements are averaged (and therefore overlapping) while the SMOS data is averaged over the whole day in the National Snow and Ice Data Center (NSIDC) 12.5 km polar stereographic grid.

The variability of the EM bird ice thickness dots illustrates the variability of the sea ice thickness within one SMOS grid cell. When averaging the EM bird retrievals by eye over the SMOS retrieval tiles, one nevertheless can recognize a quite good agreement of both retrievals along the flight track. E.g., near the turning point of the helicopter the SMOS retrievals are around 45 cm (purple), and those from the EM bird are mainly above 50 cm thickness (white) with few thin values of 10 cm and less (blue), possibly caused by leads much smaller than the SMOS footprint size (black circle in Fig. 7,

Sea ice thickness retrieval from SMOS high incident angle observations

M. Huntemann et al.

Title Page

Abstract

Introduction

Conclusions

References

Tables

Figures

⏪

⏩

◀

▶

Back

Close

Full Screen / Esc

Printer-friendly Version

Interactive Discussion



right). Since the EM bird measurement and the corresponding averages are taken along a narrow line of its footprints of 40 to 50 m width, but the SMOS footprint covers a large area, larger discrepancies in the SIT retrievals from the two instruments may occur.

For the scatter plot in Fig. 7 (left) the DGGs closest to the EM bird track are used and all EM bird measurements within 25 km distance from every of those DGG centers are averaged by using the median. With this method most EM-bird measurements are used several times according to the overlap of adjacent SMOS footprints. The correlation between the SMOS and EM bird thicknesses in Fig. 7 (left) is 0.73, and the RMSD of the two data sets is 5.1 cm.

4.3 Day-to-day differences – plausibility check

The two preceding sections have shown the limitedness in space, time and sea ice thickness of validation data available to us. Therefore, as an additional, more global consistency check the SIT difference of two consecutive days, the 20 and 21 October 2011 was investigated (Fig. 8, left). As the thermodynamic thickness growth within one day is limited, large changes are either due to drift or errors in the retrieval.

In most regions of the map the change is few cm. This is confirmed in the histogram of the differences in Fig. 8 (top right). It shows an average of 1.1 cm and a standard deviation of 3.3 cm reflecting the average ice growth throughout the Arctic. Higher variations in SIT in order of ± 10 cm occur quite seldom. They can be localized in the difference map Fig. 8 (top right). In the Beaufort Sea (75° N, 140° W), narrow parallel bands of opposite sign in SIT difference indicate sea ice drift which is confirmed by the vectors (Fig. 8, bottom right) of the sea ice drift product from the Ocean and Sea Ice Satellite Application Facility (OSI-SAF) (Lavergne et al., 2010) running perpendicular to the bands of high sea ice thickness change. Other regions of high thickness change are found near the upper limit of the retrieved sea ice thicknesses where the retrieval noise is higher, extending e.g. East of North Greenland, North of Svalbard and Franz Josef Land. The strong increase in thickness around 73° N, 133° E remains un-

explained. Concluding, this is a realistic scenario for a daily ice thickness development in the Arctic during the freeze up period.

5 Discussion and conclusions

An empirical retrieval of Sea Ice Thickness (SIT) in the freeze up period using L-band (1.4 GHz) emission of sea ice acquired by SMOS has been developed. The retrieval is trained by a Cumulative Freezing Degree days (CFDD) based model in the Kara and Barents sea during the freeze up period and uses intensity as well as polarisation difference at incidence angles between 40 and 50°.

Table 2 concludes the calibration and validation errors from the various sources. The calibration data set reveals a strong increase of the retrieval error from 3 cm for thickness below 10 cm to 16 cm in the range from 40 to 50 cm thickness. The overall average error is 9.3 cm. The two validation data set, based on MODIS and EM bird measurements respectively, confirm the tendency of better retrievals for lower ice thickness. However, as both retrieval data bases are sparse, we only give overall retrieval errors. They are 8.3 and 5.1 cm, respectively. Compared to the average error of the learning data set (9.3 cm) these values appear quite optimistic which may be explained by the small size, the homogeneity and the specific thickness distribution of the validation data sets. As the retrieval error increases with thickness, the actual error of any validation data set will depend on its thickness distribution, with higher errors for thicker ice. In Arctic-wide applications, we have to expect the average thickness towards the high end of the retrieval range of 0 to 50 cm as the ice growth speed decreases with thickness (Eq. 2). The most reliable validation data is the AWI EM bird sea ice thicknesses observations. Here, the correlation with the SMOS based thickness is 0.73 while the correlation between the MODIS and SMOS based retrievals is even higher (0.83), again supporting the suggested method.

Even though the validation studies indicate a good agreement between the three investigated data sets, further investigation to explain and understand this relationship

Sea ice thickness retrieval from SMOS high incident angle observations

M. Huntemann et al.

Title Page

Abstract

Introduction

Conclusions

References

Tables

Figures

⏪

⏩

◀

▶

Back

Close

Full Screen / Esc

Printer-friendly Version

Interactive Discussion



using a microwave emission model is desirable. This will specifically aim to quantify the additional influence of temperature, salinity and wind speed on intensity and polarisation difference.

Sensitivity studies with a radiative bulk sea ice model show little increase of intensity with increasing temperature and salinity (Maaß et al., 2013). The polarization difference also increases little with salinity, but more with temperature when it approaches melting. At higher ice thickness under freezing conditions (for which the algorithm is intended), we expect lower ice temperatures, where the temperature influence on the polarization difference again is small. Snow is nearly transparent at L band, but a noticeable effect is expected from indirect influence of snow by thermal insulation, leading to higher ice temperatures, higher polarization difference and thinner thickness retrievals (Fig. 5). We expect the strongest influences on the retrieval from temperature and snow cover, so that these influences should be investigated at highest priority. However, as the method presented here is completely empirical, the mentioned influences should automatically be included in a statistical way, e.g. a snow cover increasing statistically as the ice ages and becomes thicker. As the present study shows, even without taking these influences into account, the retrieval works within the indicated limits. Discrepancies can be expected if applied in regions with much snowfall, e.g. in the Pacific sector the the Southern Ocean.

Since SMOS radiances are quite sensitive to the incidence angle (Fig. 1) in the used incidence angle range of 40 to 50° , we are currently working on improving the retrieval by using the incidence angle as an explicit parameter. In the training, only thermodynamic and no dynamic ice growth in the Kara and Barent seas is assumed. One possibility to exclude ice thickness changes by drift from a learning data set would be to use a fast ice region, e.g., in the Laptev Sea. However, using such a data set would risk to lead to a retrieval biased towards the characteristics of undeformed ice.

Another sensor observing sea ice thickness since 2012 is Cryosat2. While SMOS is sensitive to thin ice thickness only, the altimeter Cryosat has the highest uncertainty for thin sea ice and is more accurate for thicker sea ice of more than 1 m. Comparing

Sea ice thickness retrieval from SMOS high incident angle observations

M. Huntemann et al.

Title Page

Abstract

Introduction

Conclusions

References

Tables

Figures

⏪

⏩

◀

▶

Back

Close

Full Screen / Esc

Printer-friendly Version

Interactive Discussion

Sea ice thickness retrieval from SMOS high incident angle observations

M. Huntemann et al.

Title Page

Abstract

Introduction

Conclusions

References

Tables

Figures

⏪

⏩

◀

▶

Back

Close

Full Screen / Esc

Printer-friendly Version

Interactive Discussion

- 30 Kaleschke, L., Maaß, N., Haas, C., Hendricks, S., Heygster, G., and Tonboe, R. T.: A sea-ice thickness retrieval model for 1.4 GHz radiometry and application to airborne measurements over low salinity sea-ice, *The Cryosphere*, 4, 583–592, doi:10.5194/tc-4-583-2010, 2010.
- Kaleschke, L., Tian-Kunze, X., Maaß, N., Mäkynen, M., and Drusch, M.: Sea ice thickness retrieval from SMOS brightness temperatures during the Arctic freeze-up period, *Geophys. Res. Lett.*, 39, L05501, doi:10.1029/2012GL050916, 2012.
- Källén, E.: HIRLAM Documentation Manual, System 2.5, Tech. rep., Swed. Meteorol. and Hydrol. Inst., Norrköping, Sweden., 1996.
- 5 Kerr, Y., Waldteufel, P., Wigneron, J.-P., Martinuzzi, J., Font, J., and Berger, M.: Soil moisture retrieval from space: the Soil Moisture and Ocean Salinity (SMOS) mission, *IEEE T. Geosci. Remote*, 39, 1729–1735, doi:10.1109/36.942551, 2001.
- Kruppen, T., Hedricks, S., and Haas, C.: Data report on EM-Bird ice thickness measurements for SMOSIce validation obtained during Transdrift XX, ARK XXVII/3 and SafeWin 2011 campaigns, Tech. rep., Alfred Wegener Institute for Polar and Marine Research, Bremerhaven, Germany, 2012.
- 10 Launiainen, J. and Cheng, B.: Modelling of ice thermodynamics in natural water bodies, *Cold Reg. Sci. Technol.*, 27, 153–178, 1998.
- Lavergne, T., Eastwood, S., Teffah, Z., Schyberg, H., and Breivik, L.-a.: Sea ice motion from low-resolution satellite sensors: an alternative method and its validation in the Arctic, *J. Geophys. Res.*, 115, C10032, doi:10.1029/2009JC005958, 2010.
- 15 Maaß, N., Kaleschke, L., Tian-Kunze, X., and Drusch, M.: Snow thickness retrieval over thick Arctic sea ice using SMOS satellite data, *The Cryosphere Discuss.*, 7, 3627–3674, doi:10.5194/tcd-7-3627-2013, 2013.
- 20 Mäkynen, M.: STSE-SMOS Sea Ice Retrieval Study SMOSIce WP 3 Assembly of the SMOSIce Data Base SMOSIce-DAT user manual for the validation data Deliverable D-6b Draft European Space Agency Study Contract Report Under ESTEC Contract No. 4000101476/10/NL/CT, Tech. rep., 2011.
- Mäkynen, M., Cheng, B., and Simila, M.: On the accuracy of thin-ice thickness retrieval using MODIS thermal imagery over Arctic first-year ice, *Ann. Glaciol.*, 54, 87–96, doi:10.3189/2013AoG62A166, 2013.
- 25 Mecklenburg, S., Drusch, M., Kerr, Y. H., Font, J., Martin-Neira, M., Delwart, S., Buenadicha, G., Reul, N., Daganzo-Eusebio, E., Oliva, R., and Crapolicchio, R.: ESA's soil moisture and

Sea ice thickness retrieval from SMOS high incident angle observations

M. Huntemann et al.

Title Page

Abstract

Introduction

Conclusions

References

Tables

Figures

⏪

⏩

◀

▶

Back

Close

Full Screen / Esc

Printer-friendly Version

Interactive Discussion

ocean salinity mission: mission performance and operations, *IEEE T. Geosci. Remote*, 50, 1354–1366, doi:10.1109/TGRS.2012.2187666, 2012.

30 Oliva, R., Daganzo, E., Kerr, Y. H., Mecklenburg, S., Nieto, S., Richaume, P., and Gruhier, C.: SMOS radio frequency interference scenario: status and actions taken to improve the RFI environment in the 1400–1427 MHz passive band, *IEEE T. Geosci. Remote*, 50, 1427–1439, doi:10.1109/TGRS.2012.2182775, 2012.

Sahr, K., White, D., and Kimerling, A. J.: Geodesic discrete global grid systems, *Cartogr. Geogr. Inform. Sci.*, 30, 121–134, doi:10.1559/152304003100011090, 2003.

5 Sakov, P., Counillon, F., Bertino, L., Lisæ ter, K. A., Oke, P. R., and Korablev, A.: TOPAZ4: an ocean-sea ice data assimilation system for the North Atlantic and Arctic, *Ocean Sci.*, 8, 633–656, doi:10.5194/os-8-633-2012, 2012.

Spreen, G., Kaleschke, L., and Heygster, G.: Sea ice remote sensing using AMSR-E 89-GHz channels, *J. Geophys. Res.*, 113, C02S03, doi:10.1029/2005JC003384, 2008.

10 Tonboe, R. T., Dybkjaer, G., and Høyer, J. L.: Simulations of the snow covered sea ice surface temperature and microwave effective temperature, *Tellus A*, 63, 1028–1037, doi:10.1111/j.1600-0870.2011.00530.x, 2011.

425 Uden, P., Rontu, L., Järvinen, H., and Lynch, P.: HIRLAM-5 scientific documentation, available at: <http://citeseerx.ist.psu.edu/viewdoc/summary?doi=10.1.1.6.379%4>, 2002.

Weeks, W.: *On Sea Ice*, University of Alaska Press, 2010.

Yu, Y. and Rothrock, D. A.: Thin ice thickness from satellite thermal imagery, *J. Geophys. Res.*, 101, 25753–25766, doi:10.1029/96JC02242, 1996.

Sea ice thickness retrieval from SMOS high incident angle observations

M. Huntemann et al.

Title Page

Abstract

Introduction

Conclusions

References

Tables

Figures

◀

▶

◀

▶

Back

Close

Full Screen / Esc

Printer-friendly Version

Interactive Discussion



Table 1. Parameters for fit function in Eqs. (3) and (4).

Parameter	a [K]	b [K]	c [cm]	d
I_{abc}	234.1	100.2	12.7	–
Q_{abcd}	44.8	19.4	24.1	2.1

Sea ice thickness retrieval from SMOS high incident angle observations

M. Huntemann et al.

Table 2. Retrieval Characteristics from learning and independent validation data sets. r correlation coefficient.

Data set	thickness range [cm]	RMSD [cm]	r
CFDD (learning)	0–10	3.4	
	10–20	7.3	
	20–30	9.1	
	30–40	13.8	
	40–50	16.0	
	average	0–50	9.3
MODIS	0–50	8.3	0.82
EM bird	0–50	5.1	0.73

Title Page

Abstract

Introduction

Conclusions

References

Tables

Figures

⏪

⏩

◀

▶

Back

Close

Full Screen / Esc

Printer-friendly Version

Interactive Discussion

Sea ice thickness retrieval from SMOS high incident angle observations

M. Huntemann et al.

Title Page

Abstract

Introduction

Conclusions

References

Tables

Figures

⏪

⏩

◀

▶

Back

Close

Full Screen / Esc

Printer-friendly Version

Interactive Discussion

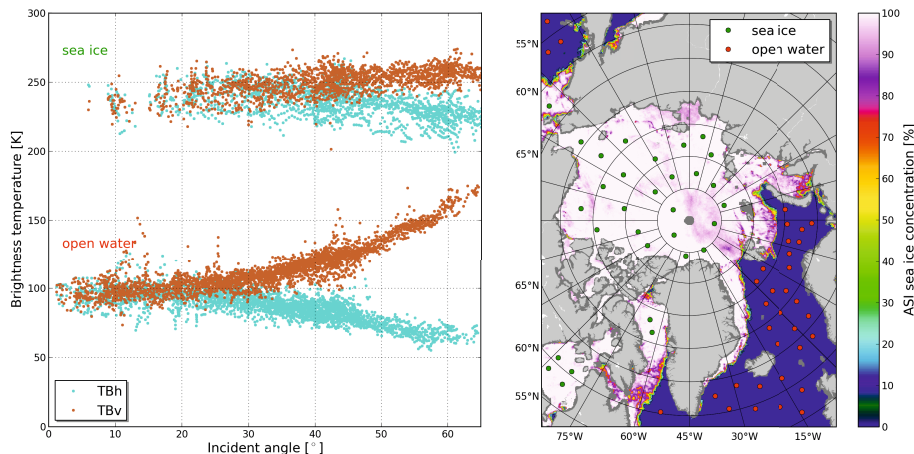


Fig. 1. Testing large area of brightness temperatures throughout the whole Arctic area from 20 April 2012. Right: ice concentration from SSMIS and test areas for sea ice (green bullets) and open water (red bullets). Left: the corresponding brightness temperature dependence on the incident angle.

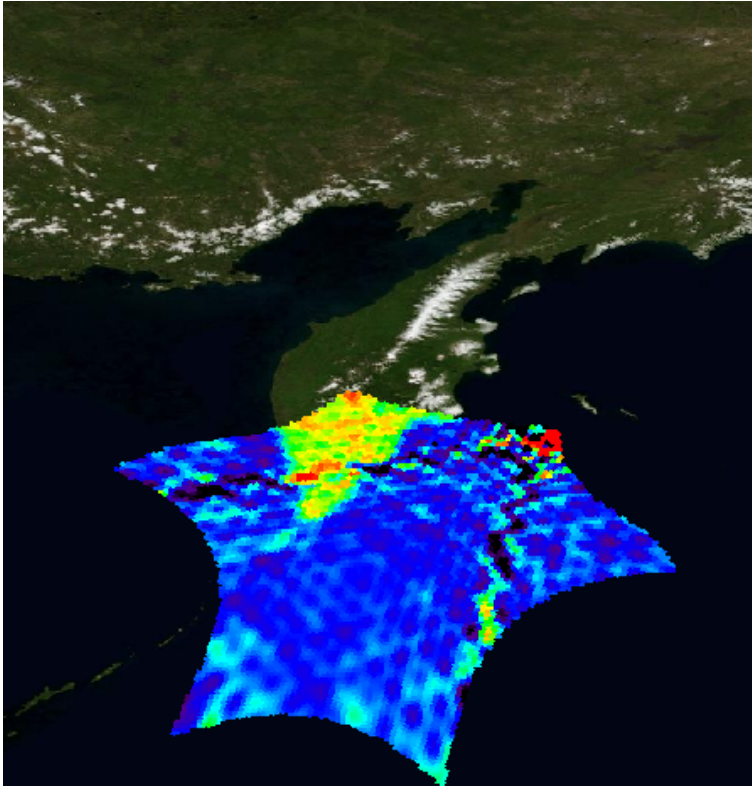


Fig. 2. A SMOS snapshot of Kamchatka and the Sea of Okhotsk as taken by MIRAS. The red area in the upper right of the snapshot represents high brightness temperatures due to RFI. In addition it produces ringing structures because of the inverse Fourier transform like reconstruction of the image. The color scale ranges from 100 K to 300 K.

Sea ice thickness retrieval from SMOS high incident angle observations

M. Huntemann et al.

Title Page

Abstract Introduction

Conclusions References

Tables Figures

⏪ ⏩

◀ ▶

Back Close

Full Screen / Esc

Printer-friendly Version

Interactive Discussion



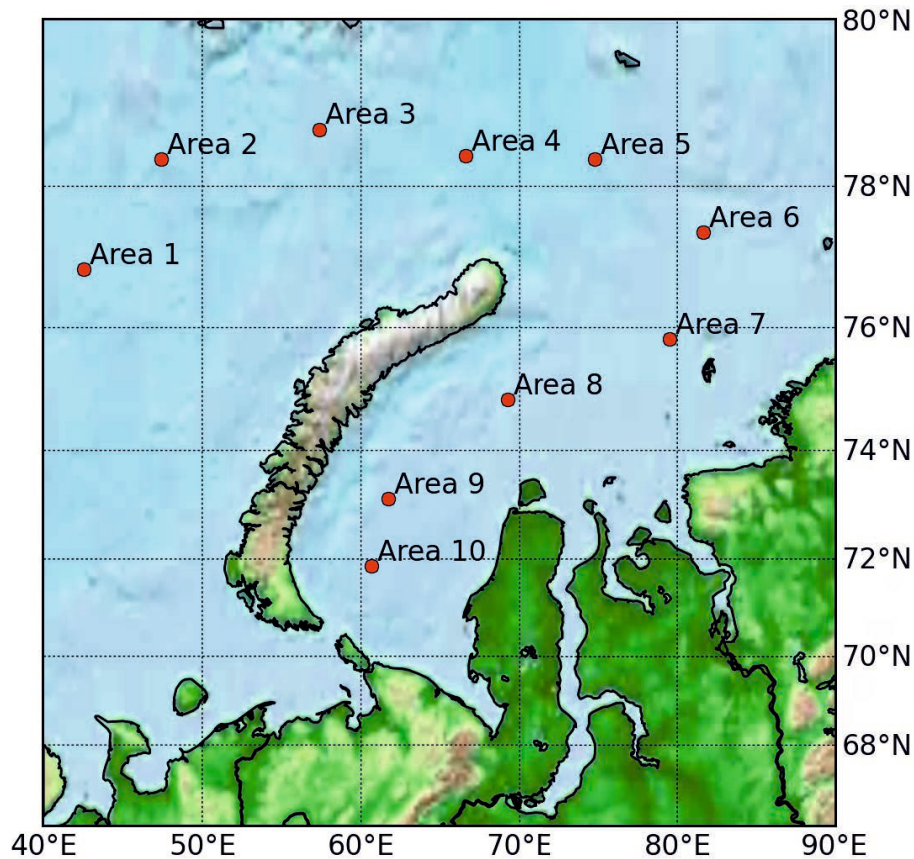


Fig. 3. Location of training areas.

Sea ice thickness retrieval from SMOS high incident angle observations

M. Huntemann et al.

Title Page	
Abstract	Introduction
Conclusions	References
Tables	Figures
◀	▶
◀	▶
Back	Close
Full Screen / Esc	
Printer-friendly Version	
Interactive Discussion	



Sea ice thickness retrieval from SMOS high incident angle observations

M. Huntemann et al.

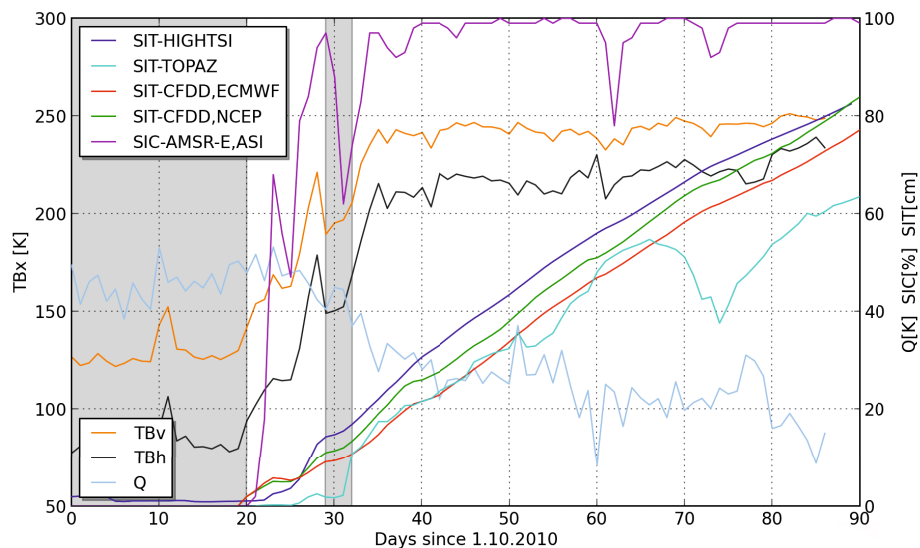


Fig. 4. SIT from training Area 7 (for location see Fig. 3) from TOPAZ, HIGHTSI, NCEP, ECMWF, Sea Ice Concentration (SIC) from ASI (AMSR-E) and SMOS brightness temperatures. Left Y-Axis for TB_h and TB_v , right Y-Axis for Q , all SITs and SIC; shaded areas are excluded for retrieval training.

Title Page

Abstract

Introduction

Conclusions

References

Tables

Figures

⏪

⏩

◀

▶

Back

Close

Full Screen / Esc

Printer-friendly Version

Interactive Discussion

Sea ice thickness retrieval from SMOS high incident angle observations

M. Huntemann et al.

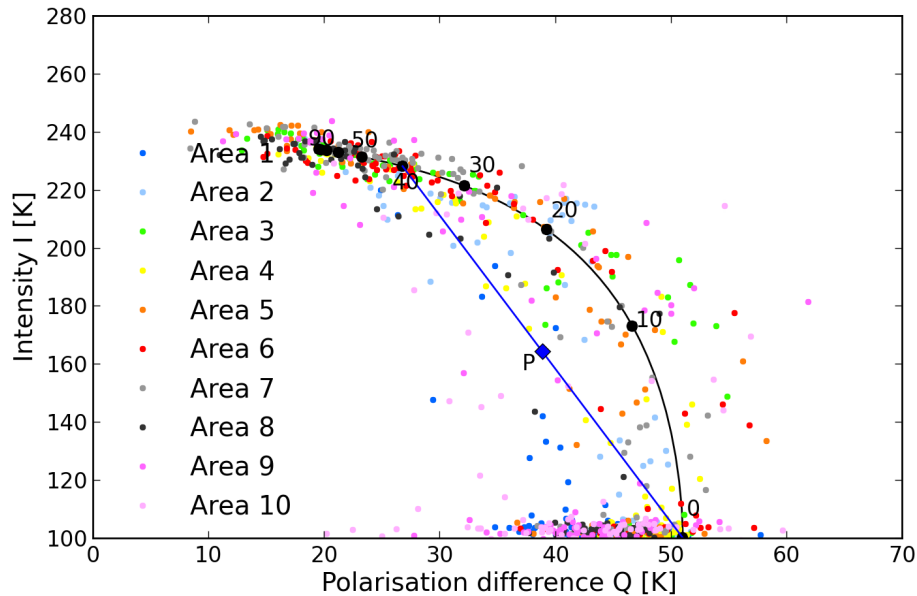


Fig. 5. Retrieval curve of SIT from I and Q . Dot colors belong to different regions (see Fig. 3). Numbers at the curve mark the retrieved SIT in cm. Observation Point P can be synthesized by observing thicknesses of 0 and 40 cm (blue line) in one footprint.

Title Page

Abstract

Introduction

Conclusions

References

Tables

Figures

◀

▶

◀

▶

Back

Close

Full Screen / Esc

Printer-friendly Version

Interactive Discussion

Sea ice thickness retrieval from SMOS high incident angle observations

M. Huntemann et al.

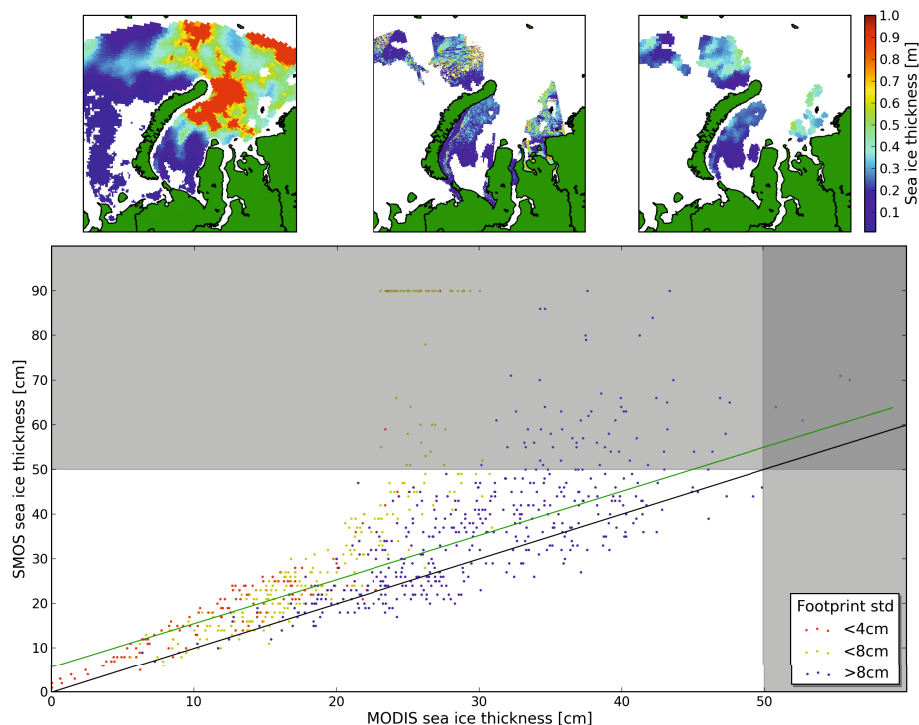


Fig. 6. Comparison between SMOS (top left) and MODIS (top center) retrieved SIT for 4 December 2010 in the Kara Sea. The valid MODIS data after averaging to the SMOS footprint size (top right). The scatter plot of MODIS and SMOS (bottom). Regression line (green): $y = 0.986x + 5.70$, RMSD = 8.3 cm, correlation 0.83.

Title Page

Abstract Introduction

Conclusions References

Tables Figures

⏪ ⏩

⏴ ⏵

Back Close

Full Screen / Esc

Printer-friendly Version

Interactive Discussion



Sea ice thickness retrieval from SMOS high incident angle observations

M. Huntemann et al.

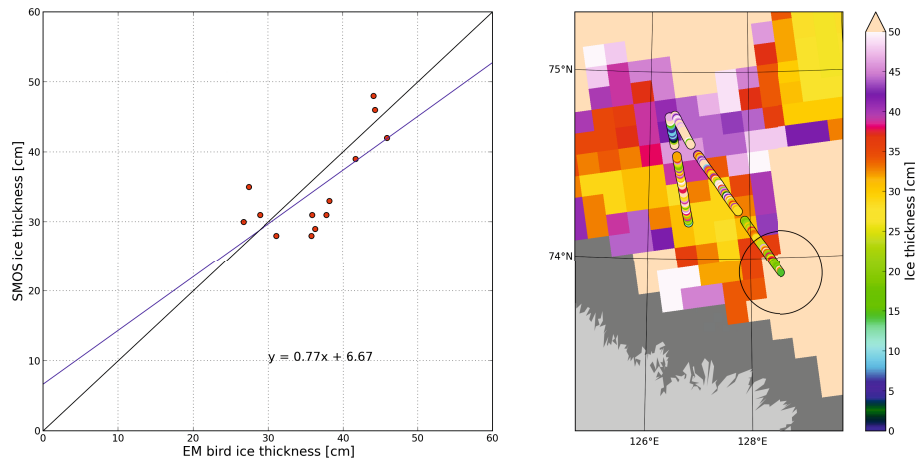


Fig. 7. Comparison of EM Bird and SMOS SIT. (right) Location of EM bird flight of 20 April 2012 (circles) median over 250 measurements and SMOS SIT (tiles). The large circle indicates the average size of a SMOS footprint. (left) Scatter plot of EM bird vs. SMOS SIT retrieval. Blue: regression line. RMSD between the data set 5.1 K, correlation 0.73.

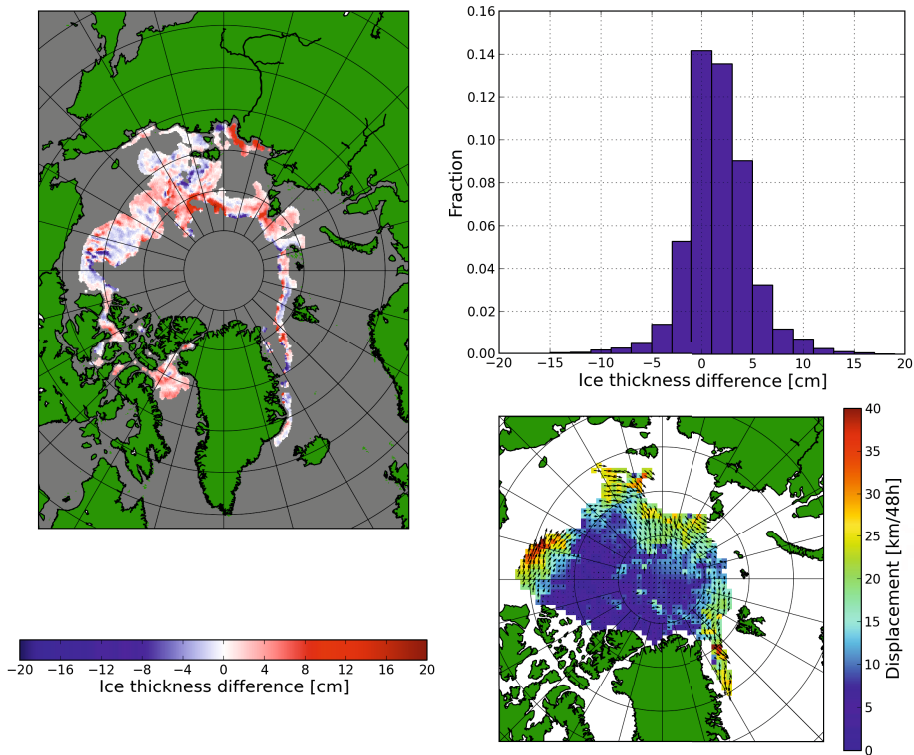


Fig. 8. Difference map of SMOS SIT retrieval from 20 to 21 October 2011 in the ice growth phase (left). Areas of open water and areas where the retrievals 50+ cm flag is set are excluded. Histogram of day to day change from 20 to 21 October 2011 (top right). OSI-SAF sea ice displacement product from 19 to 21 Oct 2011 (bottom right).

Sea ice thickness retrieval from SMOS high incident angle observations

M. Huntemann et al.

Title Page

Abstract Introduction

Conclusions References

Tables Figures

⏪ ⏩

⏴ ⏵

Back Close

Full Screen / Esc

Printer-friendly Version

Interactive Discussion

